Silicon nanopowder as diffuse rear reflector for silicon solar cells

S. Schäfer,[1,2] F. Haase,[1] R. Peibst,[1,3] and R. Brendel[1,4]
[1]*Institute for Solar Energy Research Hamelin (ISFH), Am Ohrberg 1, D-31860 Emmerthal, Germany*
[2]*Laboratory of Nano and Quantum Engineering (LNQE), Leibniz Universität Hannover, Schneiderberg 32, D-30167 Hannover, Germany*
[3]*Institute for Electronic Materials and Devices, Leibniz Universität Hannover, Schneiderberg 32, D-30167 Hannover, Germany*
[4]*Institute of Solid-State Physics, Leibniz Universität Hannover, Appelstrasse 2, D-30167 Hannover, Germany*

(Received 27 March 2017; accepted 21 July 2017; published online 3 August 2017)

Highly efficient solar cells require minimized recombination and maximized optical absorption. We apply Si nanopowder with a median particle size of 500 nm to the rear side of poly-Si on oxide (POLO) passivated Si wafers that have a planar front side. The enhanced optical absorption consists of a useful component from the wafer and useless absorption by the Si pigments and the poly-Si layer. We derive and successfully apply an analytical model that accounts for both contributions and for the light trapping that is caused by light scattering at the nanopowder layer. We measure and model that this rear side increases the photogenerated current density by 1.3 mA/cm^2 for a 140 μm-thick planar cell. We compare the performance of the Si-pigmented diffuse rear side reflectors (PDR) with reflectors using random pyramids (RPs) and POLO junctions. We find that for full surface coverage by Si nanopowder, the better surface passivation compensates for an inferior optical performance of a PDR when compared to RP. *Published by AIP Publishing.*
[http://dx.doi.org/10.1063/1.4997183]

I. INTRODUCTION

Lambertian light trapping is a widely used benchmark for good light trapping. A surface is called to be fully Lambertian if complete randomization of the direction of light propagation occurs after transmission through and reflection at this surface.[1,2] In today's monocrystalline silicon solar cells, light trapping is achieved by wet alkaline etching of randomly[3] or regularly arranged[4] pyramids. The optical absorption of pyramidally textured structures approaches that of Lambertian light trapping schemes for weakly absorbed light.[5] Light trapping and reduced front reflectance outweigh efficiency-wise the detrimental effect of an increased surface recombination that comes along with the increase in the surface area.

In some cases, however, surface textures on the front side are not possible. One example for this is the Si-based tandem or multijunction devices which consist of a thin wide-band gap top cell that is monolithically grown or bonded onto a crystalline silicon bottom cell.[6–8] Growing the top cell on textured surfaces is an unsolved challenge. With a planar front side, the silicon bottom cell can be textured on the rear side to introduce light trapping.

Another challenge with pyramidal textures arises for poly-Si on oxide (POLO) junctions.[9,10] We found that carrier recombination of the POLO junctions is significantly higher on pyramidally textured surface with (111)-oriented facets than on planar (100) surfaces.[11] This holds for both polarities. While these junctions show low recombination current densities of $J_0 = 1$–4 fA/cm^2 on planar (100) surfaces for n^+- and p^+-type POLO junctions, respectively, these values were found to be about one order of magnitude higher on random pyramid (RP) surfaces.[9,11]

Both challenges are addressed by a light trapping scheme on the rear side that is electronically planar and optically rough. Such light trapping schemes were realized by nanostructuring of the rear side passivating layer,[12] by plasmonic particles,[13] and by pigmented diffuse rear side reflectors (PDR).[14] Compared to the other approaches, a PDR has the advantage that it is easy-to-apply and does not require nanostructuring and/or chemical vapor deposition equipment.

A PDR consists of two components with different refractive indices n_i: the pigment (i = p) and the matrix material (i = m) [see Fig. 1(b)]. The size of the pigments, the volumetric fraction, and the ratio of the refractive indices of the pigment and the matrix determine the wavelength dependent scattering efficiency of the PDR (see Ref. 14 and references therein). For maximizing the scattering efficiency, the difference $|n_p - n_m|$ between the refractive indices of the pigment and matrix should be high. However, one has to keep in mind that a matrix material with a low index will decrease the probability for entering and leaving the matrix material from and into the silicon wafer, respectively.

PDR surfaces that have a higher refractive index of the pigment than of the matrix are named type-I PDR in this paper, while the opposite case is named type-II PDR. TiO_2 nanoparticles, either in a pure form[15,16] or as "white paint," in combination with a binding medium,[14,17–19] are an example of type-I PDRs. TiO_2 has a high refractive index of $n_p \sim 2.7$. The reported gain in the extracted current density of a 200 μm-thick and planar Si cell with a white paint PDR over a cell with a specular rear reflector amounted to 0.8 mA/cm^2.[19] In the case of type-II PDRs, silica microspheres with $n_p \sim 1.5$ were used as low-n pigments and the

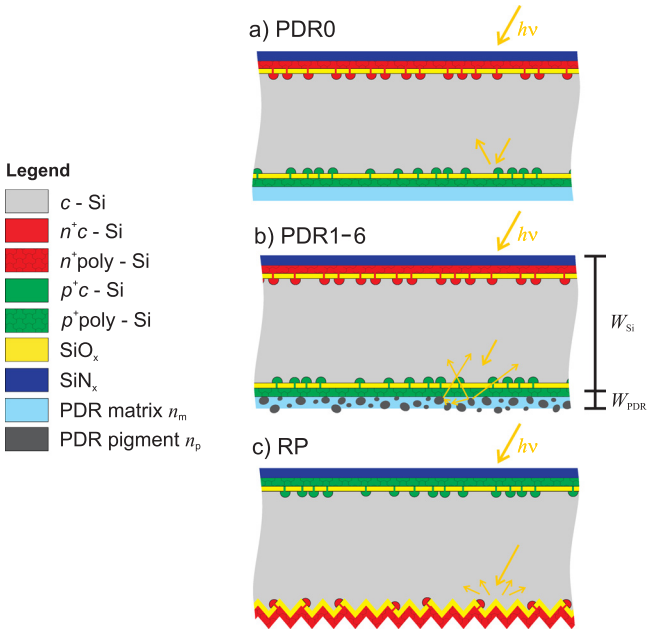

FIG. 1. A sketch of the investigated sample structures. The samples are solar cell precursors with carrier selective POLO junctions. (a) The sample PDR0 with no pigments $c_p = 0$ in the rear reflector, (b) the samples PDR1 through PDR6 have a varying pigment concentration c_p in the pigmented diffuse rear reflector (PDR), and (c) the sample RP with a random pyramid texture and the electron selective contact on the rear side. The PDR consists of the pigments, here Si nanopowder, with refractive index n_p and the surrounding matrix, here a spin-on SiO_x with refractive index n_m.

matrix, either amorphous titanium oxide ($n_m \sim 2.38$)[20] or *n*-type poly-Si ($n_m \sim 3.5$)[21] as the component with the higher refractive index. In the latter case, the gain over a 200 μm-thick planar cell amounted to 1.4 mA/cm^2.[21]

In this contribution, we introduce silicon nanopowder ($n_p \sim 3.5$) as an effective, high-index scattering pigment in a type-I PDR. We apply nanopowder of varying Si particle concentrations to Si wafers with carrier selective POLO junctions. We show that this new kind of PDR not only outperforms previous type-I PDR but can also show a better electro-optical performance than random pyramids in combination with an n^+-type POLO junction.

II. EXPERIMENTAL

A. Sample preparation

Figure 1 shows the three sample structures considered in this paper. We start with double side planar (140 ± 4) μm-thick and (15.6 × 15.6) cm^2-sized *n*-type Cz-Si wafers with a resistivity of 8 Ω cm. The carrier selective POLO junctions are prepared as in Ref. 22: After an RCA cleaning, the samples receive a 1.7 nm-thick thermal oxide, followed by a 30 nm-thick LPCVD intrinsic poly-Si layer. The poly-Si layers are doped via ion implantation. The boron implantation dose is 2×10^{14} cm^{-2} for a planar surface. The phosphorous implantation dose is 2.5×10^{15} cm^{-2} for a planar surface and 4.25×10^{15} cm^{-2} for a surface textured with random pyramids. The post-implantation annealing takes place at 950 °C for 30 min for all sample types. During annealing, the thin interface oxide locally breaks up and allows dopant diffusion from the poly-Si into the *c*-Si as shown in Fig. 1.[23,24] The planar front side of the three samples is covered by a PECVD antireflection coating (ARC) that consists of 70 nm silicon nitride with a refractive index of 1.9 ($SiN_{x,\ n=1.9}$) at a wavelength of 633 nm. All samples have an *n*-type and a *p*-type POLO junction as required for a working solar cell. All samples (a) to (c) are laser cut into (2.5 × 2.5) cm^2 pieces.

The PDR is prepared as follows: We use a commercially available silicon nanopowder[25] with a median particle size (D50) of 500 nm as a pigment. The purity of the powder is stated to be 99.9 at. %. We mix 5 ml isopropanol (IPA) with varying amounts of Si nanopowder to study the influence of the pigment concentration c_p on the matrix. The concentrations are $c_p = 0.03$–0.34 g/ml. Table I lists and describes the investigated samples with their respective pigment concentration used. All dispersions are sonicated for 5 min prior to spin-coating. Spin-coating takes place in two steps: the first step uses a rotation speed of 600 rpm for 10 s during which 1 ml of the dispersion is dropped onto the sample. The second step uses a speed of 1000 rpm for 5 s without further dropping. The IPA evaporates when placing the samples onto a hotplate (100 °C). In the second spin-coating procedure with identical parameters, we deposit 1 ml of a siloxane-based SiO_2 precursor as a matrix material onto the pigments.[26] We determine the refractive index of the matrix material to be $n_m = 1.39$ at 633 nm by ellipsometry. The annealing after the second spin-coating step takes place at 220 °C for 2 min.

We deposit the PDR on the hole selective contact [see Fig. 1(b)] which implies that the electron selective contact is on the planar front side. Having a perovskite-Si tandem device in mind, we motivate this choice by the strong absorption of the hole transporting material in perovskite solar cells[27] that should not directly face the sun. In any case, changing the polarity has a negligible impact on the photogenerated current density for poly-Si layers that are thinner than 30 nm.[28] The relevant reference sample with random pyramids on the rear side [see Fig. 1(c)] uses the electron selective contact on the textured side to show optimum performance of the Si cell.[9]

B. Characterization tools

We study the morphology of the PDR samples using an electron microscope (S-4800 from Hitachi). We use a

TABLE I. List of the investigated samples with specified light trapping scheme from Fig. 1, macroscopic thickness W_{Si} and Si pigment concentration c_p. We measure absorption and transmission spectra as well as the effective minority carrier lifetimes of all samples.

Name	Light trapping scheme	W_{Si} (μm)	c_p (g/ml)
PDR0	Figure 1(a)	140	0
PDR1	Figure 1(b)	140	0.03
PDR2	Figure 1(b)	140	0.07
PDR3	Figure 1(b)	140	0.09
PDR4	Figure 1(b)	140	0.15
PDR5	Figure 1(b)	140	0.24
PDR6	Figure 1(b)	140	0.34
RP	Figure 1(c)	160	…

spectrophotometer (Cary 5000 from Varian) to measure absorption and transmission spectra. Absorption is measured with the samples being positioned in an integrating sphere of 150 mm in diameter. The absorption spectra are measured under an angle of incidence of 8°, while the transmission spectra are taken at normal incidence. We measure the minority carrier lifetimes by the dynamic infrared lifetime mapping (dyn-ILM) technique[29] at a carrier injection level that results from an illumination intensity of 1 sun. The ideality factor and the saturation current density of POLO-passivated reference samples are obtained from injection dependent photoconductance decay measurements using a WCT-120 from Sinton instruments.[30]

III. RESULTS

A. Morphology of PDR

Figure 2 shows SEM micrographs of a 15°-tilted cross-sectional view of the rear surface of the four samples PDR0, PDR1, PDR4, and PDR6. The thickness of the resulting PDR is (1.5 ± 1) μm. The pigment concentration c_p influences the packing density of the particles rather than the thickness of the PDR. Thus, while sample PDR1 exhibits uncovered parts of the surface, the Si pigments fully cover the surface of sample PDR6. The SEM micrographs also show that the bulk crystalline silicon (c-Si) has a slight roughness induced by etching the saw damage. While this is disadvantageous from the point of modelling, this roughness will be present in the low-cost Si material of real solar cells.

B. Impact of PDR on the absorption spectrum

Figure 3(a) displays the measured absorption spectra (round full symbols) of the samples PDR1, PDR4, and PDR5 (see Table I). These samples differ in pigment concentrations c_p of the PDR. We focus on the wavelength region between 900 nm and 1300 nm where light absorption in Si becomes small, and where, therefore, the pigments enhance the measured absorption. In addition, the sample PDR0 with $c_p = 0$ g/ml (round empty symbols) is displayed as a reference. The magenta dashed line is the simulated absorption of a Lambertian light trapping scheme for a wafer that is 140 μm thick and has the measured front and rear reflection of the planar Si wafer.[31]

From the spectra in Fig. 3(a), we learn the following: (i) The PDR increases the absorption when compared to the sample PDR0. (ii) This increase in absorption increases with the pigment concentration c_p. (iii) The sample PDR0 shows absorption above a wavelength of 1200 nm which cannot be attributed to the absorption in the Si wafer. This absorption is due to the highly doped poly-Si layers. (iv) The samples PDR1 to PDR6 show a higher absorption above 1200 nm than PDR0. This extra absorption is due to parasitic absorption in the PDR and absorption enhancement in the POLO junctions.

C. Optical model for separating A_{Si} and A_{PDR}

The parasitic absorption in the PDR and the poly-Si at the front and the rear side is combined in the measure A_{PDR} and does not contribute to the external quantum efficiency in a solar cell. In order to calculate the useful absorption A_{Si} in the Si wafer from the measured total absorption $A_{meas} = A_{Si} + A_{PDR,}$ we apply an optical model. The optical model is illustrated in Fig. 4 and is similar to that presented in Ref. 32. We distinguish fully specular (black lines) and fully diffusive light (red lines). We consider two stacked silicon layers: a planar Si wafer and a second thin layer with a rough rear side that shall mimic the combined impact of the poly-Si layer and the PDR. The two layers have a thickness of W_i, a refractive index of n_i, and an absorption coefficient of α_i (i = Si, PDR). Simplifying the real situation, we assume that (i) scattering takes place only at the rear side of the PDR, (ii) both Si and the PDR have the same refractive index ($n_{Si} = n_{PDR} = n$), i.e., there is no reflection at the interface, and (iii) the absorption coefficient in the PDR α_{PDR} is constant in the range of 900–1400 nm, i.e., $\alpha_{PDR} W_{PDR} = a_{PDR}$. The validity of these assumptions will be discussed later in this section after having fully described the model.

The model considers 12 optical power fluxes I_{ijkl}. The index i distinguishes fluxes in the wafer (i = Si) and the PDR (i = PDR) or at their interface (i = x). Index j distinguishes the top (j = t) from the bottom (j = b) of the two layers, while the index k marks upward (k = u) or downward (k = d) propagation. The last index l distinguishes specular (l = s) from diffusive (l = d) light. Light that impinges onto any of the two surfaces of the layer stack has the probability T_m to be transmitted through the front (m = f) or the back surface (m = b), respectively. As the rear side of the PDR is rough, we assume a probability Λ_b for specularly impinging light to become fully randomized after reflection. We term the probability Λ_b the Lambertian character of the PDR. The diffusive light, drawn in red in Fig. 4, partly suffers total internal reflection that limits the transmission probability to $T_m\,(1/n_i)^2$ at the silicon/air interface. The symbol $T_{i,s} = \exp(-\alpha_i W_i)$ denotes the

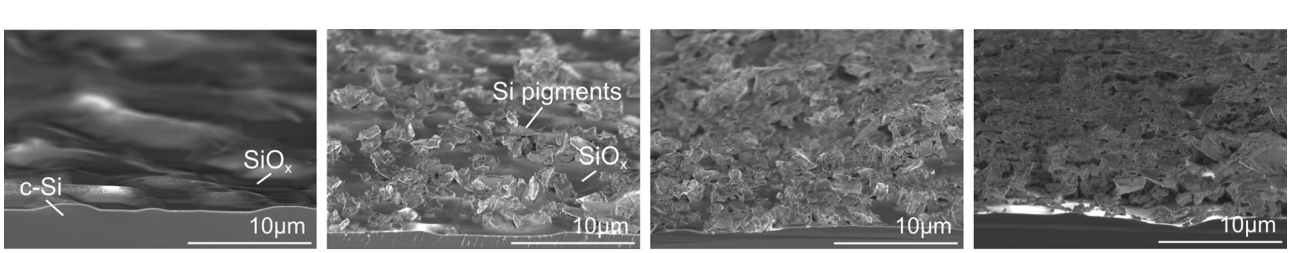

FIG. 2. SEM micrographs of the tilted cross-sections of the PDR rear side with Si pigments embedded in a spin-on SiO_x with varying pigment concentrations c_p. The thickness of the PDR is (1.5 ± 1) μm.

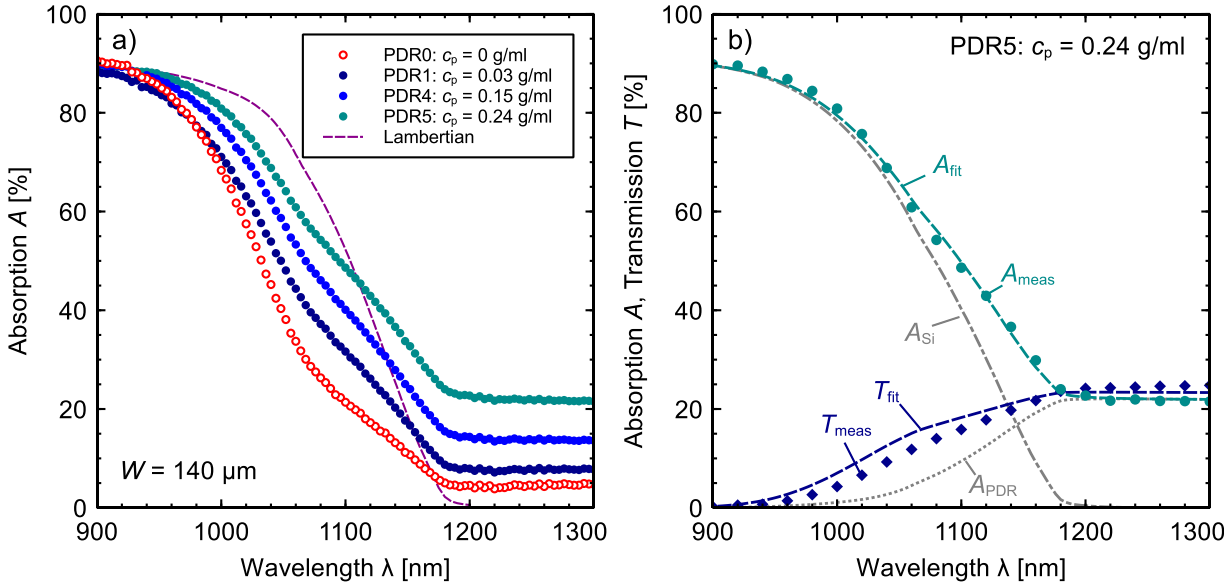

FIG. 3. (a) The absorption spectra of the sample PDR0 (empty circles), samples with different pigment concentrations c_p (full circles), and a simulated absorption for Lambertian light trapping without an external reflector (dashed line). (b) The application of the optical model and the measured A_{meas} (full circles), fitted $A_{fit} = A_{Si} + A_{PDR}$ and separated absorptions of the silicon layer A_{Si} and the PDR/poly-Si layers A_{PDR} as well as the measured (full squares) and fitted transmissions, T_{meas} and T_{fit}, respectively.

transmittance for specular light propagating normally to the surfaces through the wafer. In contrast, the symbol $T_{i,d}$ denotes the transmittance of fully randomized light and reads[33,34]

$$T_{i,d}(\alpha_i W_i) = \exp(\alpha_i W_i)(1-\alpha_i W_i) + (\alpha_i W_i)^2 \int_{\alpha_i W_i}^{\infty} t^{-1}\exp(-t)dt. \quad (1)$$

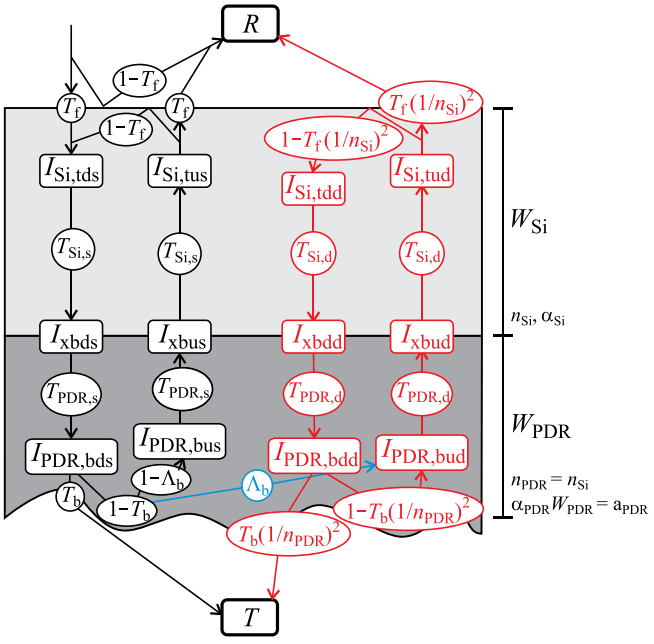

FIG. 4. A schematic of the 12 optical power fluxes I_{ijkl} in the two absorbing layers silicon and PDR. The black and red colors denote the specular and fully randomized optical power flux. The blue arrow symbolizes the power transfer from the specular channel to the diffusive channel according to the Lambertian character Λ_b. Equations (A1)–(A16) can be set up by collecting the factors to the respective power flux. The ratio of the thicknesses is not to scale.

The equations for the 12 intensities I_{ijkl} are listed in the Appendix. We solve for the absorptions in the Si layer A_{Si} and in the PDR and the poly-Si A_{PDR}, as well as for the total transmission T_{fit} of the stack that we will later fit to the experimental data. The result is

$$A_{Si} = \frac{T_f}{(B(T_f-1)+1)C} \times \Big(T_{PDR,d} T_{Si,s} T_{PDR,s} \Lambda_b n^2 \times (T_b-1)(T_{Si,d}-1)\Big(T_{Si,d}(T_f-n^2)-n^2\Big) - (T_{Si,s}-1)\Big(\frac{B}{T_{Si,s}}+1\Big)C\Big), \quad (2)$$

$$A_{PDR} = \frac{T_f T_{Si,s}}{(B(T_f-1)+1)C} \times \Big(T_{PDR,s}\Lambda_b n^2 (T_b-1) \times (T_{PDR,d}-1)\Big(T_{Si,d}^2 T_{PDR,d}(T_f-n^2)-n^2\Big) - (T_{PDR,s}-1)\Big(\frac{B}{T_{Si,s}^2 T_{PDR,s}}+1\Big)C\Big), \quad (3)$$

for the absorptions and

$$T_{fit} = \frac{T_f T_b T_{Si,s} T_{PDR,s}}{B(T_f-1)+1} \times \Big(1 - \frac{T_{Si,d}^2 T_{PDR,d}^2 \Lambda_b (T_b-1)(T_f-n^2)}{C}\Big), \quad (4)$$

for the transmission. We have used the abbreviations

$$B = T_{Si,s}^2 T_{PDR,s}^2 (T_b\Lambda_b - T_b - \Lambda_b + 1), \quad (5)$$

$$C = T_{Si,d}^2 T_{PDR,d}^2 (T_b - n^2)(T_f - n^2) - n^4. \quad (6)$$

Note that the purpose of this model is not to understand the functioning of the PDR. For this, it would be necessary to

model the light scattering in individual particles, e.g., by solving the Maxwell equations.[35] This is, however, clearly beyond the scope of this paper. The purpose of our model is to extract the useful absorption $A_{Si} = A_{meas} - A_{PDR}$ from the measured absorption. To do so, we introduce only three degrees of freedom into the model: a degree of absorption a_{PDR} by the PDR and the POLO junction, a degree of light scattering Λ_b by the PDR, and a degree of the reflectance $(1–T_b)$ of the PDR.

Assumption (i) is justified since the PDR is much thinner than the Si wafer. For the absorption in the Si wafer, it does not matter where exactly the direction of light propagation is randomized in the PDR. Assumption (ii) is motivated by the fact that a non-zero reflection at the Si/PDR interface can be accounted for by a reduced value of T_b in combination with an enhanced value for a_{PDR} and/or Λ_b. We experimentally verified assumption (iii) by measuring a PDR applied to a glass substrate which shows a constant absorption of $(25 \pm 5)\%_{abs}$ in the wavelength range of 950–1300 nm.

As stated earlier, this model has only three free parameters: Λ_b, a_{PDR}, and T_b. We obtain these parameters by simultaneously fitting the measured absorption spectrum A_{meas} and the measured transmission spectrum T_{meas}. The values for Λ_b and T_b are forced to lie between 0 and 1. Figure 3(b) displays the spectra that were measured and fitted for sample PDR5. For all samples, the parameters for the best fit are given in Table II. The absorption coefficient in the PDR a_{PDR} scales linearly with the parasitic absorption J^*_{PDR} [see Eq. (7)] for the samples PDR0 through PDR6. The Lambertian character Λ_b is above 0.9 for all samples. The main reason for this is that the bulk material itself has a certain surface roughness (see Fig. 2). This is apparently sufficient to make the long-wavelength absorption Lambertian-like. The absorption enhancement here mainly manifests itself in the transmission probability T_b that decreases with the pigment concentration c_p. Note that actually the *scattering* in the PDR induces a change in T_b and that this change must not lead to the conclusion that the PDR loses its benefit when combined with an external mirror or backsheet. The supplementary material discusses the impact of the PDR when combined with an external mirror. We consider the agreement of measurement and fit in Fig. 3(b) for both the absorption and the transmission spectrum to be a strong support of the three modelling assumptions.

D. Impact of PDR on photogeneration in the Si wafer

With the fitted parameters Λ_b, a_{PDR}, and T_b, we extract the useful absorption in the silicon layer $A_{Si}(\lambda)$ using Eq. (2). From this, we calculate the photogenerated current density J^*_{Si} in the silicon wafer by

$$J^*_{Si} = \frac{q}{hc}\int_{700nm}^{1400nm} \lambda I(\lambda) A_{Si}(\lambda) d\lambda. \tag{7}$$

Here, $I(\lambda)$, q, h, and c denote the spectral irradiance of the AM1.5g spectrum,[36] the elementary charge, Planck's constant, and the speed of light in vacuum, respectively. Replacing the absorption in Eq. (7) by the measured absorption A_{meas} or by the parasitic absorption, A_{PDR} gives the corresponding current densities J^*_{meas} and J^*_{PDR}, respectively. We determine the share of absorbed photons in the Si wafer S and multiply it with J^*_{meas} to obtain the current density

$$J^*_{Si} = J^*_{meas} \times S = J^*_{meas} \times \frac{J^*_{Si}}{J^*_{Si} + J^*_{PDR}}, \tag{8}$$

which contains the uncertainty of the measurement of J^*_{meas}. J^*_{Si} on the right-hand side of Eq. (8) is obtained by Eq. (7) with the modeled A_{Si}. From now on and throughout the paper, J^*_{Si} is defined by Eq. (8). Table II lists these three quantities J^*_{meas}, S, and J^*_{Si} for the measured samples and the difference $J^*_{meas} - J^*_{fit}$ is a measure for the accuracy of the model. Figure 5 shows a plot of the relative optical gain

$$\Delta_x = \frac{J^*_x(c_p)}{J^*_x(0)} - 1 \tag{9}$$

of the samples PDR1 through PDR6 over the sample PDR0. The gains of the measured current densities (x = meas) and useful absorption in silicon (x = Si) are represented in squares and circles in Fig. 5 for the PDR samples, respectively. The gain in photogeneration Δ_{meas} according to Eq. (9) reaches a value of $(15 \pm 0.8)\%$ for a particle concentration of $c_p = 0.24$ g/ml. The parasitic loss J^*_{PDR} also depends on c_p and reduces Δ_{meas} to $\Delta_{Si} = (7.6 \pm 0.8)\%$. This corresponds to an absolute gain of (1.30 ± 0.01) mA/cm^2 as listed in Table II. The share of the parasitic absorption $(1 - \Delta_{Si}/\Delta_{meas})$ is $(49.6 \pm 4.6)\%$ of the measured optical gain for the samples with Si particles. Literature values that were

TABLE II. Overview of the results. The measured effective minority carrier lifetime and the fit parameters from the optical model. The next three columns state the photogenerated current density for wavelengths between 700 and 1400 nm of the measured absorption spectra J^*_{meas} [see Eq. (7)], and the factor S represents the share of the photons absorbed in the Si wafer and the product J^*_{Si} [see Eq. (8)] of both values. The last column gives the absolute difference $\Delta J^* = J^*_{meas} - J^*_{fit}$.

Name	τ_{eff} (μs)	Λ_b	a_{PDR}	T_b	J^*_{meas} (mA/cm^2)	$S = \frac{J^*_{Si}}{J^*_{Si}+J^*_{PDR}}$	J^*_{Si} (mA/cm^2)	$J^*_{meas} - J^*_{fit}$ (mA/cm^2)
PDR 0	640 ± 50	1	0.00498	0.632	18.91	0.976	18.47	0.12
PDR 1	480 ± 30	0.931	0.00534	0.424	19.43	0.963	18.71	0.02
PDR 2	508 ± 21	0.972	0.00701	0.398	19.97	0.951	18.98	0.04
PDR 3	401 ± 12	0.968	0.00589	0.354	20.02	0.954	19.09	0.03
PDR 4	475 ± 27	0.922	0.00779	0.293	20.77	0.939	19.51	0.02
PDR 5	520 ± 29	0.944	0.0111	0.197	21.76	0.908	19.77	0.02
PDR 6	518 ± 27	1	0.00985	0.227	21.26	0.916	19.48	0.03
RP	269 ± 14	1	0.00455	0.207	23.06	0.954	22.00	0.07

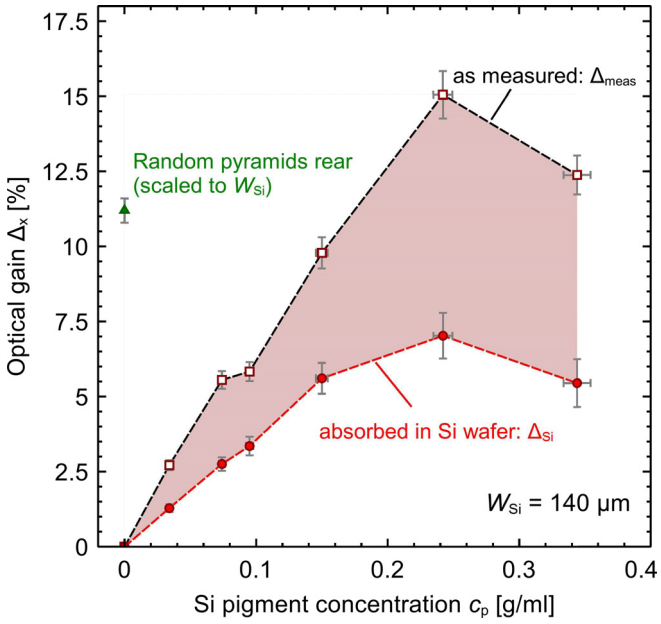

FIG. 5. The calculated relative gain in photogenerated current density according to Eq. (8) for the absorption as measured (square symbols) and corrected by the parasitic absorption (round symbols) depending on the concentration of Si pigments in the PDR. The shaded area corresponds to the parasitic absorption. The triangular symbol marks the reference with random pyramids on the rear side triangular.

derived from comparing spectrophotometric measurements and external quantum efficiencies of 200 μm-thick solar cells employing a PDR showed a smaller share of 30%–33% parasitic absorption.[19,21] This difference can most likely be attributed to the thinner wafers and the absorption enhancement in the poly-Si layers.

Figure 5 also shows a symbol for the sample RP with random pyramids [see Fig. 1(c)]. The thickness of the sample is $W_{Si} = 160\,\mu$m, and we scale its J^*_{Si} by a factor $20.86/22.44 = 0.93$ which is the ratio of the photogenerated current densities of a Lambertian light trapping scheme for absorber thicknesses of 140 and 160 μm, as calculated by Eq. (7). The triangle in Fig. 5 symbolizes this scaled Δ_{Si} value. The useful photogeneration of random pyramids outperforms our PDR structure by 0.69 mA/cm^2 in the investigated wavelength region.

The gain in photogeneration Δ_{Si} approaches a limit above a Si pigment concentration of $\sim$0.2 g/ml. Our interpretation is that the Si pigments fully cover the surface of the wafer from the limit concentration, as indicated in the SEM micrographs of Fig. 2. Therefore, Δ_{Si} increases with c_p until full area coverage is reached and then saturates.

IV. THE IMPACT OF PDR ON SURFACE PASSIVATION AND COMPARISON TO RANDOM PYRAMIDS

In this section, we answer the question whether it can be useful to replace random pyramids on the rear side of a Si bottom cell with a Si powder PDR. For this, we extend the optical characterization by carrier lifetime measurements to evaluate whether the PDR deteriorates the surface passivation quality. The measured effective lifetimes τ_{eff} for the samples are listed in Table II. The Si nanopowder seems to have an impact on the passivation quality as the τ_{eff} of the sample PDR1 through 6 declines compared to the sample PDR0 with no pigments. A possible reason for this is the damage of the passivation layer through sample handling. Any mechanical external force on the surface, e.g., from tweezers, gets distributed over the contact area between the surface and the pigments. The sample RP, however, has a lower τ_{eff} than all samples with a planar POLO junction at the rear side. This corresponds to total recombination current densities of $J_0 = (43 \pm 5)$ fA/cm^2 for the samples with the planar rear side and $J_0 = (60 \pm 2)$ fA/cm^2 for the sample with pyramids on the rear side.[37] We calculate a quality factor

$$QF = \frac{J^*_{Si}(c_p) \times V^*_{oc}(c_p) \times FF_0\left(v^*_{oc}(c_p)\right)}{J^*_{Si}(0) \times V^*_{oc}(0) \times FF_0\left(v^*_{oc}(0)\right)} \qquad (10)$$

for each sample.[38] Here, J^*_{Si} symbolizes the photogenerated current density in silicon, and V^*_{oc} stands for the implied open circuit voltage. FF_0 symbolizes the fill factor that only depends on the normalized voltage $v^*_{oc} = V^*_{oc}/mV_{th}$, with the thermal voltage $V_{th} = 25.85$ mV and the ideality m.[39] We find an ideality of $m \approx 0.7$ by fitting the one-diode equation to the photoconductance decay measurements (not shown).[30] The value for the ideality indicates that the samples are in high injection and Auger limited.[40] For calculating the J^*_{Si} values, we change the lower integration limit in Eq. (7) to 300 nm to include the whole convertible solar spectrum. We determine

$$V^*_{oc} = V_{th} \ln\left(\frac{1}{n_i^2}\left(\left(\frac{J^*_{Si}}{qW}\tau_{eff} + \frac{N_D}{2}\right)^2 - \left(\frac{N_D}{2}\right)^2\right)\right), \qquad (11)$$

from the intrinsic carrier concentration n_i, here assumed to be $n_i = 8.7 \times 10^9\,\text{cm}^{-3}$,[40] where q is the elementary charge, W_{Si} is the absorber thickness, τ_{eff} is the measured effective minority carrier lifetime at an illumination intensity of 1 sun, and N_D is the doping density.

Figure 6 shows the resulting quality factor QF of the investigated samples. The J^*_{Si} value of the RP sample is scaled

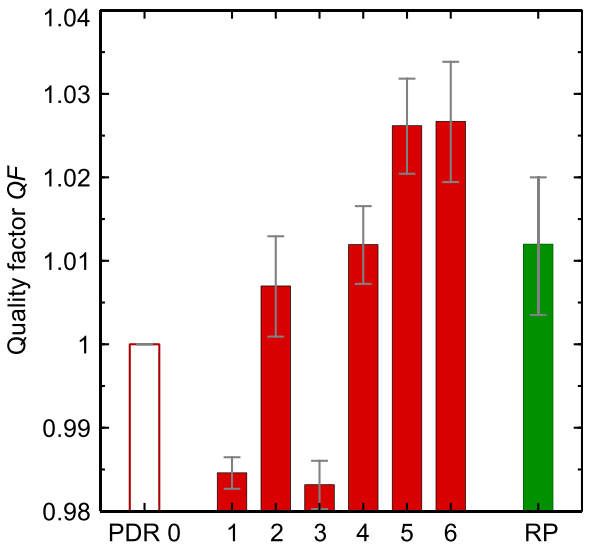

FIG. 6. The quality factor QF as defined by Eq. (10) for the POLO passivated samples with the light trapping schemes from Figs. 1(a)–1(c).

to a thickness of 140 μm as described earlier. We find that all samples differ by less than ±3%. Two samples with PDR have a higher QF than the random pyramid sample RP. However, the difference is as large as the measurement inaccuracy. Thus, the benefit of the better surface passivation by the planar POLO junction compensates the disadvantage in the optical performance for the samples investigated here. The importance of the surface passivation quality can be seen for the samples PDR1 and PDR3 which have a lower QF as the sample with no additional light trapping. The best PDR sample PDR6 has a QF that is $\Delta QF = (2.7 \pm 0.7)\%$ higher than the PDR0 sample with no Si pigments. The sample with random pyramids as light trapping scheme has a $\Delta QF = (1.2 \pm 0.8)\%$.

V. SUMMARY AND DISCUSSION

In this paper, we have introduced Si nanopowder as a scattering pigment in a diffuse rear reflector (PDR). We have studied the impact of the pigment concentration c_p on the gain in photogeneration. The pigments introduce light scattering which enhances useful light absorption and parasitic absorption. We have separated both with an analytical optical model. For an absorber thickness of $W_{Si} = 140\,\mu$m, the PDR leads to a 1.3 mA/cm^2 higher photogenerated current density compared to the sample with no light trapping scheme. This optical performance is higher than that of previous reported type-I PDRs that rely on TiO_2 as a scattering pigment. The light trapping performance of the PDR is inferior to that of random pyramids on the rear side of a cell with a planar front side. This disadvantage, however, can be compensated by a better surface passivation when compared to an n^+-type POLO contact on pyramidal textures. It is known that n^+-POLO contacts allow for lower recombination current densities on pyramidal textures.[9] This suggests that the PDR has an advantage when compared to a p^+-type POLO contact on the pyramidal texture. At this stage of our research, we suggest the PDR to be applied after metallization of the rear as is common to previously reported type-I PDRs. We do not expect the metal fingers to impair the PDR deposition due to the excellent adhesion between the pigments and the substrate. However, the deposition parameters and/or technique have to be adapted for certain substrate morphologies to achieve full surface coverage of the PDR. Whether the PDR could also be contacted directly, e.g., by making the pigments and/or the matrix conductive has yet to be determined.

This makes the Si nanopowder PDR on POLO junctions an interesting approach if for one or the other reason the cells front side should remain flat. Note that the deposition of the Si nanopowder PDR is straightforward, and no vacuum or lithography equipment is required.

SUPPLEMENTARY MATERIAL

See supplementary material for a characterization of the Si nanopowder PDR in combination an external mirror.

ACKNOWLEDGMENTS

The authors thank Yevgeniya Larionova, Renate Winter, and Bianca Gehring for processing the POLO samples and Michael Rienäcker for fruitful discussions. This work was funded by the German Federal Ministry for Economic Affairs and Energy under Contract Nos. 0325702 (POLO) and 0325827A (26+).

APPENDIX: TWO-LAYER OPTICAL MODEL

The 12 different power fluxes I_{ijkl} in Fig. 4 can be set up by following the arrows towards the respective power flux and collecting the multipliers on these paths. For normally incident light with intensity 1, they read

$$I_{Si,tds} = T_f + (1 - T_f) I_{Si,tus}, \tag{A1}$$

$$I_{xbds} = T_{Si,s} I_{Si,tds}, \tag{A2}$$

$$I_{Si,tus} = T_{Si,s} I_{xbus}, \tag{A3}$$

$$I_{xbus} = T_{PDR,s} I_{PDR,bus}, \tag{A4}$$

$$I_{PDR,bds} = T_{PDR,s} I_{xbds}, \tag{A5}$$

$$I_{PDR,bus} = (1 - \Lambda_b)(1 - T_b) I_{PDR,bds}, \tag{A6}$$

$$I_{Si,tdd} = 1 - T_f (1/n_{PDR})^2 I_{Si,tud}, \tag{A7}$$

$$I_{xbdd} = T_{Si,d} I_{Si,tdd}, \tag{A8}$$

$$I_{xbud} = T_{PDR,d} I_{PDR,bud}, \tag{A9}$$

$$I_{Si,tud} = T_{Si,d} I_{xbud}, \tag{A10}$$

$$I_{PDR,bdd} = T_{PDR,d} I_{xbdd}, \tag{A11}$$

$$I_{PDR,bud} = (1 - T_b)\Lambda_b I_{PDR,bds} + 1 - T_b (1/n_{Si})^2 I_{PDR,bdd}. \tag{A12}$$

Once the equation set is solved for the 12 power fluxes, Eqs. (2)–(4) are calculated by the expressions

$$A_{Si} = (1 - T_{Si,s})(I_{Si,tds} + I_{xbus}) + (1 - T_{Si,d})(I_{Si,tdd} + I_{xbud}), \tag{A13}$$

$$A_{PDR} = (1 - T_{PDR,s})(I_{xbds} + I_{PDR,bus}) + (1 - T_{PDR,d})(I_{xbdd} + I_{PDR,bud}), \tag{A14}$$

$$T_{fit} = T_b I_{PDR,bds} + T_b (1/n_{PDR})^2 I_{PDR,bdd}, \tag{A15}$$

$$R_{fit} = T_f I_{Si,tus} + (1 - T_f) + T_f (1/n_{Si})^2 I_{Si,tud}. \tag{A16}$$

[1]E. Yablonovitch and G. Cody, IEEE Trans. Electron Devices **29**, 300 (1982).
[2]A. Goetzberger, in *Proceedings of the 15th IEEE Photovoltaic Specialists Conference* (1981), p. 867.
[3]D. H. Neuhaus and A. Münzer, Adv. OptoElectron. **2007**, 24521.
[4]J. Zhao, A. Wang, P. Altermatt, and M. A. Green, Appl. Phys. Lett. **66**, 3636 (1995).
[5]P. Campbell and M. A. Green, J. Appl. Phys. **62**, 243 (1987).
[6]F. Dimroth, T. Rösner, S. Essig, C. Weuffen, A. Wekkeli *et al.*, IEEE J. Photovoltaics **4**, 620 (2014).
[7]J. P. Mailoa, C. D. Bailie, E. C. Johlin, E. T. Hoke, A. J. Akey *et al.*, Appl. Phys. Lett. **106**, 121105 (2015).
[8]S. Essig, J. Benick, M. Schachtner, A. Wekkeli, M. Hermle, and F. Dimroth, IEEE J. Photovoltaics **5**, 977 (2015).
[9]R. Peibst, Y. Larionova, S. Reiter, M. Turcu, R. Brendel *et al.*, in *Proceedings of the 32nd European Photovoltaic Solar Energy Conference and Exhibition* (2016), p. 323.

[10]J.-Y. Gan and R. M. Swanson, in *Proceedings of the 21st IEEE Photovoltaic Specialists Conference* (1990), p. 245.
[11]Y. Larionova, R. Peibst, M. Turcu, S. Reiter, R. Brendel *et al.*, in *Proceedings of the 32nd European Photovoltaic Solar Energy Conference and Exhibition* (2016), p. 452.
[12]J. Eisenlohr, N. Tucher, H. Hauser, M. Graf, J. Benick *et al.*, Sol. Energy Mater. Sol. Cells **155**, 288 (2016).
[13]F. J. Beck, A. Polman, and K. R. Catchpole, J. Appl. Phys. **105**, 114310 (2009).
[14]J. E. Cotter, R. B. Hall, M. G. Mauk, and A. M. Barnett, Prog. Photovoltaics: Res. Appl. **7**, 261 (1999).
[15]B. G. Lee, P. Stradins, D. L. Young, K. Alberi, T.-K. Chuang *et al.*, Appl. Phys. Lett. **99**, 64101 (2011).
[16]A. Basch, F. Beck, T. Söderström, S. Varlamov, and K. R. Catchpole, Prog. Photovoltaics: Res. Appl. **20**, 837 (2012).
[17]O. Berger, D. Inns, and A. G. Aberle, Sol. Energy Mater. Sol. Cells **91**, 1215 (2007).
[18]B. Lipovšek, J. Krč, O. Isabella, M. Zeman, and M. Topič, Phys. Status Solidi C **7**, 1041 (2010).
[19]F. Pfeffer, J. Eisenlohr, A. Basch, M. Hermle, B. G. Lee, and J. C. Goldschmidt, Sol. Energy Mater. Sol. Cells **152**, 80 (2016).
[20]J. Eisenlohr, J. Benick, M. Peters, B. Bläsi, J. C. Goldschmidt, and M. Hermle, Opt. Express **22**, A111 (2014).
[21]J. Eisenlohr, B. G. Lee, J. Benick, F. Feldmann, M. Drießen *et al.*, Sol. Energy Mater. Sol. Cells **142**, 60 (2015).
[22]U. Römer, R. Peibst, T. Ohrdes, B. Lim, J. Krügener *et al.*, IEEE J. Photovoltaics **5**, 507 (2015).
[23]R. Peibst, U. Römer, Y. Larionova, M. Rienäcker, A. Merkle *et al.*, Sol. Energy Mater. Sol. Cells **158**, 60 (2016).
[24]D. Tetzlaff, J. Krügener, Y. Larionova, S. Reiter, M. Turcu *et al.*, Sol. Energy Mater. Sol. Cells (in press).
[25]Sky Spring Nanomaterials, Inc., see www.ssnano.com for product and order information.
[26]B. Veith-Wolf, J. Wang, M. Hannu-Kuure, N. Chen, A. Hadzic *et al.*, Appl. Phys. Lett. **106**, 52104 (2015).
[27]M. Filipič, P. Löper, B. Niesen, S. De Wolf, J. Krč *et al.*, Opt. Express **23**, A263 (2015).
[28]S. Reiter, N. Koper, R. Reineke-Koch, Y. Larionova, M. Turcu *et al.*, Energy Procedia **92**, 199 (2016).
[29]K. Ramspeck, S. Reißenweber, J. Schmidt, K. Bothe, and R. Brendel, Appl. Phys. Lett. **93**, 102104 (2008).
[30]R. A. Sinton and A. Cuevas, Appl. Phys. Lett. **69**, 2510 (1996).
[31]R. Brendel and D. Scholten, Appl. Phys. A **69**, 201 (1999).
[32]R. Brendel, T. Dullweber, R. Peibst, C. Kranz, A. Merkle, and D. Walter, Prog. Photovoltaics: Res. Appl. **24**, 1475 (2016).
[33]R. Brendel, Jpn. J. Appl. Phys. Part 1 **40**, 4431 (2001).
[34]A. Luque and G. L. Araújo, *Solar Cells and Optics for Photovoltaic Concentration* (Adam Hilger, Bristol, 1989), p. 508
[35]C. F. Bohren and D. R. Huffman, *Absorption and Scattering of Light by Small Particles* (John Wiley & Sons, 2008).
[36]C. A. Gueymard, Sol. Energy **76**, 423 (2004).
[37]D. E. Kane and R. M. Swanson, in *Proceedings of 18th IEEE Photovoltaic Specialists Conference* (1985), p. 578.
[38]S. Schäfer, C. Gemmel, S. Kajari-Schröder, and R. Brendel, IEEE J. Photovoltaics **6**, 397 (2016).
[39]M. A. Green, Sol. Cells **7**, 337 (1982).
[40]A. Richter, M. Hermle, and S. W. Glunz, IEEE J. Photovoltaics **3**, 1184 (2013).